A Generalized Class of Stationary Frame-Current Controllers for Grid-Connected AC–DC Converters

A Generalized Class of Stationary Frame-Current Controllers for Grid-Connected AC–DC Converters

J. George Hwang, *Student Member, IEEE*, Peter W. Lehn, *Senior Member, IEEE*, and Manfred Winkelnkemper, *Member, IEEE*

***Abstract*—Within power systems, high-power pulsewidth-modulated ac–dc converters are used in flexible ac transmission systems controllers and for interfacing renewable energy sources to the grid. These converters traditionally employed PI controllers designed in the synchronous dq-frame with decoupling of d and q axes. Recently, stationary $\alpha\beta$-frame proportional-resonant (PR) controllers have been proposed. Though both types of control are suitable for the regulation of three-phase converters, the PR controller displays steady-state and dynamic behavior that differs significantly from that of decoupled dq-frame controllers. This paper derives a stationary frame controller that is the exact equivalent of the commonly used synchronous frame controller with ωL decoupling. The new stationary frame "PRX2" controller consists of a proportional (P), a resonant (R), and two cross-coupling components. The PRX2 controller offers identical transient and steady-state performance and has the same frequency response as the decoupled synchronous frame PI controller. Unlike other stationary frame controllers containing resonant components, the PRX2 controller is unique because it contains a cross-coupling feedback component, which accounts for the behavior of the ωL decoupling branches present in synchronous frame controllers. It is shown that ignoring this decoupling component greatly increases the controller's sensitivity to frequency variation. Numerous stationary frame controllers, including the common PR controller, may be derived from the general PRX2 controller.**

***Index Terms*—Active rectifier, complex transfer functions, current control, resonant control, stationary frame, synchronous frame, voltage-source converter (VSC).**

I. Introduction

AN EVER-GROWING number of high-power pulsewidth-modulated (PWM) ac–dc converters are finding application within power systems. Traditionally, control of these converters was carried out by using the synchronous dq reference frame [1]–[6]. By modeling the converter system in the dq-frame, the control problem is simplified. In place of tracking three 60-Hz reference signals for currents i_a, i_b, i_c, only two dc reference signals need to be tracked, namely, i_d and i_q. This is easily accomplished through the use of conventional proportional-integral (PI) control [2], [5]–[8].

One side-effect of performing control in the synchronous frame is that the dq-frame converter model contains two cross-coupling terms linking the d- and q-axis dynamics. It is common practice to cancel these ωL cross-coupling terms via feedback before carrying out the design of the PI regulators [3]–[7]. Thus, the complete dq-frame converter controller contains the following components:

1) ωL decoupling branches on each of the d and q-axes;
2) PI regulators on each of the d and q-axes.

By including these two elements, the synchronous frame controller is able to achieve fast dynamic response and zero steady-state tracking error under balanced operating conditions. The behavior of these controllers is well documented [1].

In the past decade, researchers have explored use of proportional-resonant (PR) regulators for control of ac-dc converters using the stationary $\alpha\beta$-frame [4], [9]–[12]. Based on the "internal model principle" first proposed by Francis and Wonham [13], a PR regulator can offer fast dynamic response and zero steady-state tracking error for sinusoidal signals. This avoids the need to convert the system variables into the dq-frame and the associated need for a phase-locked loop (PLL) [14]. The following benefits of stationary frame controllers have been identified in the literature:

- elimination of the PLL removes errors that would be brought upon by synchronization problems [11];
- in microgrids, aerospace applications, or remote networks, the elimination of the PLL means the converter can never lose synchronization with the grid, thus stationary frame controllers will never trip due to synchronization failure caused by extreme frequency or phase variations [15];
- elimination of abc-to-dq and dq-to-abc frame transformations, thus significantly reducing overall computation burden [10] on control hardware and driving down system cost (this plays a role in smaller systems where control costs make up a significant percentage of total cost (e.g., photovoltaic grid interface converters));
- improved response to unbalanced faults [15];
- improved grid current waveforms when interface inductors are not perfectly balanced between the phases;
- significant reduction in dc ripple under grid imbalance, leading to reduced dc capacitor sizing [16];
- better suited for single-phase systems, where the dq-transformation is difficult to apply [11].

From a grid imbalance perspective, synchronous frame control is entirely able to deal with negative-sequence currents and the accompanying harmonic power [17], [18]. For example,

Manuscript received March 18, 2009; revised August 18, 2009. Current version published September 22, 2010. Paper no. TPWRD-00225-2009.

J. G. Hwang is with the Department of Electrical Engineering and Computer Science, Massachusetts Institute of Technology, Cambridge, MA 02139 USA (e-mail: ghwang@mit.edu).

P. W. Lehn is with the Department of Electrical and Computer Engineering, University of Toronto, Toronto, ON M5S 3G4, Canada (e-mail: lehn@ecf.utoronto.ca).

M. Winkelnkemper is with ABB Switzerland Ltd., Turgi CH-5300, Switzerland (e-mail: manfred.winkelnkemper@ch.abb.com).

Color versions of one or more of the figures in this paper are available online at http://ieeexplore.ieee.org.

Digital Object Identifier 10.1109/TPWRD.2010.2045136

Jiang and Ekström [17] utilize a feedforward scheme to help mitigate the effects of grid imbalance in dq-frame-controlled converters. On the other hand, stationary frame resonant controllers, such as the PR controller, employ feedback rather than feedforward to deal with unbalance. This makes them more robust to sensor imbalance, interface reactor imbalance, and other disturbances.

Though the synchronous and stationary frame controllers can be used for ac–dc converter control, their dynamic and steady-state behaviors differ [14]. Some inroads have been made to clarify the mapping between the dq-frame and $\alpha\beta$-frame transfer functions [10], [19]. To date, however, no stationary frame controller exists that is dynamically equivalent to the conventional dq-frame controller with ωL decoupling branches.

This paper builds upon the work of Zmood *et al.* [9]–[11] and Yuan *et al.* [12] to develop a precise stationary frame equivalence of the complete synchronous frame controller—including the influence of the two PI regulators and the two ωL decoupling branches. The objectives of this paper are twofold: first, to enhance our understanding of the mapping between synchronous and stationary frame controllers, and second, to address performance limitations of stationary frame controllers compared to their synchronous frame counterparts.

In Section II, the equivalence is developed by transforming the synchronous frame ac–dc converter plant and its associated synchronous frame controller, including ωL decoupling branches, into the stationary frame. Unlike previous approaches that transform only the PI regulator transfer function into the stationary frame [9]–[11], here rotational operators are employed to transform the entire system model into the stationary frame [19]. As a result, a new stationary frame PRX2 controller is identified that consists of a proportional (P), resonant (R), and two cross-coupled ($\mathrm{X}control$ and $\mathrm{X}feedback$) components.

In Section III, the efficacy of the PRX2 controller is demonstrated via simulation and experimental results. Furthermore, several other viable controllers that are derived by neglecting various feedback branches in the PRX2 controller, including the common PR controller, are examined.

One limitation of conventional PR controllers is their high sensitivity to system frequency. Specifically, their tracking ability degrades rapidly as the system frequency deviates from its nominal value. In contrast, the proposed PRX2 controller is shown in Section IV to be highly robust to variations in frequency, similar to that of a synchronous frame controller. This makes the PRX2 controller suitable for a broader class of applications than existing PR controllers. Use of resonant controllers for applications ranging from microgrids to aerospace may now be explored through the use of the PRX2 controller.

Throughout this paper, $\alpha\beta$-frame is the stationary frame derived from the abc-frame via the Clarke transformation, while the dq-frame refers to the synchronous frame. Details may be found in [20].

II. Grid-Connected AC–DC Modeling and Control

The grid connected ac–dc converter voltage-source converter (VSC) system is shown in Fig. 1. The $\alpha\beta$-frame controller

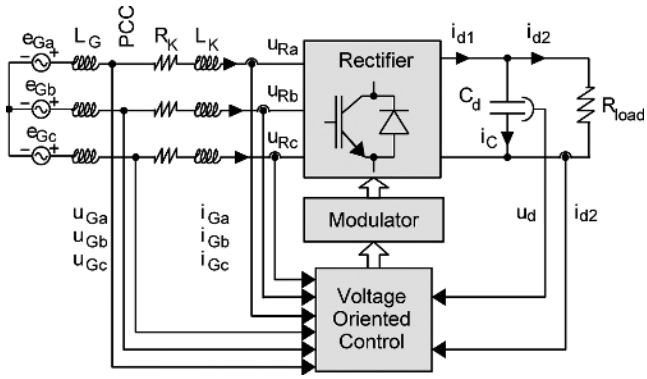

Fig. 1. Block diagram of a controlled ac–dc converter with dc load.

is derived by using a two-step process. First, the converter is modeled in the dq-frame and the controller is derived by using voltage-oriented control (VOC) [2] per Fig. 1. Second, the entire model—plant and controller—is transformed to the $\alpha\beta$-frame via rotational operators [19] per Fig. 2. The resulting system is then trivially broken into controller and plant dynamics.

A. Modeling and Control in the Synchronous Frame

The control equations for the grid-connected ac–dc converter system are derived from the dq-axes grid (1a), (1b) and dc-link (2) in the synchronous frame [21]

$$\frac{d}{dt}i_{Gd} = -\frac{R_K}{L_K}i_{Gd} + \omega i_{Gq} - \frac{1}{L_K}u_{Rd} + \frac{1}{L_K}u_{Gd} \quad (1a)$$

$$\frac{d}{dt}i_{Gq} = -\frac{R_K}{L_K}i_{Gq} - \omega i_{Gd} - \frac{1}{L_K}u_{Rq} + \frac{1}{L_K}u_{Gq} \quad (1b)$$

$$\frac{d}{dt}u_d = \frac{3}{2C_d}\cdot\frac{u_{Gd}i_{Gd}}{u_d} - \frac{1}{C_d}i_{d2} \quad (2)$$

where L_K, R_K, and C_d are the converter interface inductance, resistance, and dc-link capacitance, and the system frequency is $\omega_N = 377$ rad/s. The ac-side signals u_{Gd} and u_{Gq}, i_{Gd} and i_{Gq}, and u_{Rd} and u_{Rq} are the d- and q-axis point of common coupling (PCC) voltage, converter line current, and converter ac terminal voltage, respectively. The dc-side signals u_d and i_{d2} are the dc- link voltage and load current, respectively. In (2), it is assumed that the d axis is synchronized to the PCC voltage via a PLL so that $u_{Gq} = 0$ and the losses in the line resistance R_K and the converter are neglected. The converter switching frequency is well above the fundamental frequency of the grid it is connected to.

To independently control i_{Gd} and i_{Gq}, the following standard decoupling scheme is utilized to create separate, identical d, and q-axis single input-single output systems [4], [22]

$$u_{Xd} = u_{Gd} - u_{Rd} + \omega L_K i_{Gq}, \quad (3a)$$

$$u_{Xq} = u_{Gq} - u_{Rq} - \omega L_K i_{Gd}. \quad (3b)$$

An inner current loop regulates the d and q-axis currents via a PI regulator of the form

$$G_{PI}(s) = \frac{sK_P + K_I}{s}. \quad (4)$$

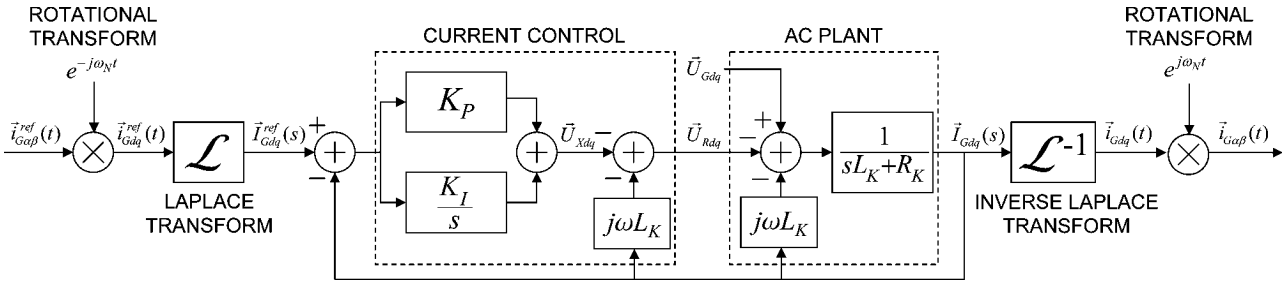

Fig. 2. Synchronous dq-frame-current control loop with synchronous-to-stationary frame rotational transform operators at the input and output.

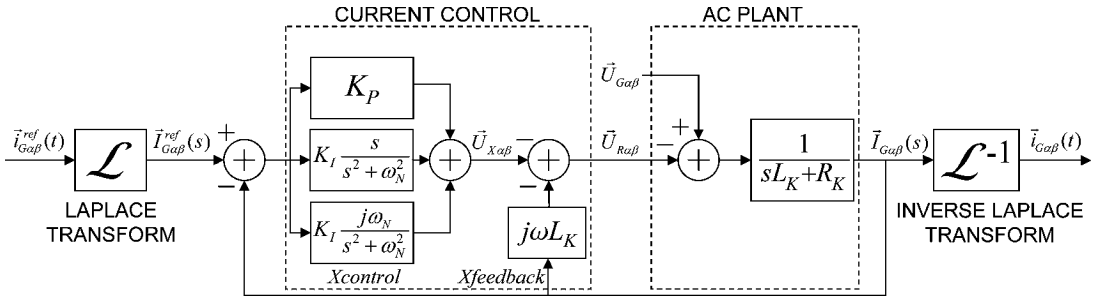

Fig. 3. Stationary $\alpha\beta$-frame-current control model equivalent to the synchronous dq-frame model with rotational transform operators shown in Fig. 2.

The d-axis current is used to regulate the dc-link voltage and exchange real power with the dc load/source. It is further discussed in Section II-C. The q-axis current supplies reactive power. The proportional and integral gain values used are $K_P = 0.564$ and $K_I = 113$.

B. Stationary Frame Control via Rotational Reference Frame Transformation

Resonant controllers typically employ a proportional (P) and a resonant (R) term, taking the form of (5) [11]

$$G_{PRstat}(s) = K_{Pstat} + K_{Rstat}\frac{s}{s^2+\omega_N^2}. \tag{5}$$

In [9]–[11], Zmood *et al.* suggest that the values of the proportional and integral gains K_P and K_I, used in a dq-frame PI controller should be the same as those used for the proportional and resonant gains K_{Pstat} and K_{Rstat}, respectively, in the $\alpha\beta$-frame PR controller; however, the equivalence of the full models is not shown.

Instead of adopting a controller of the predefined form given in (5), it is proposed that a stationary frame controller be derived by applying synchronous-to-stationary frame rotational operators to the synchronous frame system model [19] of Fig. 2. By block manipulation and pulling the input rotational operator through the current loop to the output, a control loop with only stationary frame voltages and currents can be realized as in Fig. 3.

The control and system dynamics are easily separated from one another as also indicated in Fig. 3. Focusing on the resulting stationary frame controller, it contains both the transfer function

$$\begin{aligned} G_{PRXcontrol}(s) &= K_P + K_I\frac{1}{s-j\omega_N} \\ &= K_P + K_I\frac{s}{s^2+\omega_N^2} + K_I\frac{j\omega_N}{s^2+\omega_N^2} \end{aligned} \tag{6}$$

plus an additional $\mathrm{X}_{feedback} = j\omega L_K$ branch that operates on the feedback current alone. This branch is the remnant of the synchronous frame decoupling scheme of (3a) and (3b). The controller contains a complex gain component, called the X$control$ branch, that cross-couples the α and β current errors. The X$control$ branch arises due to the generalized integrator which is centered about $s = j\omega_N$ [12] and, therefore, contains a complex number in the denominator, as shown in the first line of (6).

The complete controller, including X$control$ and X$feedback$ branches, is called the PRX2 controller. Gains of the PRX2 controller K_P and K_I are the same gains calculated for the dq-frame PI controller, as suggested by Zmood *et al.* [9]–[11]. The derivation of the mathematical equivalence of the dq-frame and $\alpha\beta$-frame models is detailed in the Appendix.

C. DC-Link Voltage Regulation

The dc-link voltage is regulated by using a PI controller of the form

$$G_{\mathrm{dc}}(s) = \frac{sK_{Pdc} + K_{Idc}}{s}. \tag{7}$$

The PI control gains used for the dc-link voltage controller are $K_{Pdc} = 0.37$ and $K_{Idc} = 29$.

The stationary $\alpha\beta$-frame reference currents, $i_{G\alpha}^{\mathrm{ref}}$ and $i_{G\beta}^{\mathrm{ref}}$, are produced by using the output of the dc-link voltage controller, namely i_{Gd}^{ref}, and the $\alpha\beta$-frame PCC grid voltage space vector $\vec{u}_{G\alpha\beta}$. To achieve near unity power factor, the $\alpha\beta$-frame reference currents are:

$$i_{G\alpha} = i_{Gd}^{ref} \times \frac{u_{G\alpha}}{\sqrt{u_{G\alpha}^2 + u_{G\beta}^2}} \tag{8a}$$

$$i_{G\beta} = i_{Gd}^{\mathrm{ref}} \times \frac{u_{G\beta}}{\sqrt{u_{G\alpha}^2 + u_{G\beta}^2}}. \tag{8b}$$

TABLE I
CONTROLLER VARIATIONS STUDIED

Controller	Description
dq-frame	Synchronous frame with PI regulators and ωL decoupling branches
PRX2	Resonant with both X$control$ and and X$feedback$ branches
PRX$control$	Resonant with X$control$ branch only
PRX$feedback$	Resonant with X$feedback$ branch only
PR	Resonant with no cross-coupling branches

TABLE II
PARAMETERS OF SIMULATION/EXPERIMENTAL SETUP

Parameter	Abbr.	Value
Rated/base apparent power	S_N	2 kVA
Grid voltage (line-neutral)	e_G	120 V
Grid inductance	L_G	100 μH
Input line resistance	R_K	0.15 Ω
Input line inductor	L_K	2.5 mH
dc link capacitance	C_d	70 μF
dc link voltage	u_d	375 V
Switching frequency	f_{sw}	6 kHz

III. IMPACT OF CROSS-COUPLING TERMS

The PRX2 controller contains two cross-coupling branches that do not appear in the conventional stationary frame PR controller of (5). Specifically, these are the cross-coupling branches X$control$ and X$feedback$ shown in Fig. 3.

To fully understand the effect each cross-coupling branch has on the frequency- and time-domain characteristics of the stationary frame PRX2 controller, different controllers with variations on the inclusion of the two cross-coupling branches are analyzed. The controllers studied are listed and described in Table I. Note the synchronization of the measured voltages and currents into the dq-frame was done via a PLL. The simulation and experimental system configuration is shown in Fig. 1 with parameters of the system given in Table II. All simulations were performed by using Matlab, Simulink, and Plecs.

A. Frequency-Domain Analysis

Figs. 4 and 5 display the complex open- and closed-loop responses of the controllers given in Table I. The open-loop response of the PRX2 controller, the PRX$control$, PRX$feedback$, and PR controllers display infinite gain and zero phase lag at 60 Hz. This leads to unity gain and zero phase lag in the closed-loop responses—otherwise known as zero steady-state error at 60 Hz.

The effect of removing the X$feedback$ branch, as is done in the PRX$control$ controller, is clearly seen by comparing closed-loop responses in Fig. 5(a) and (b). At frequencies neighboring 60 Hz, the PRX$control$ controller experiences a faster and larger deviation from unity gain. Therefore, it is more sensitive to frequency deviation.

The effect of removing the X$control$ branch, as is done in the PRX$feedback$ controller, is clearly seen by comparing the open-loop responses in Fig. 4(a) and (c). Exclusion of the X$control$ branch produces an infinite gain and zero phase lag at -60 Hz, as was shown by Yuan *et al.* [12]. This allows the PRX$feedback$ controller to fully regulate -60-Hz (negative sequence) and $+60$-Hz (positive sequence) current components. This is seen in the closed-loop response of Fig. 5(c) as well.

The effect of removing both cross-coupling branches, as is the case for the PR controller, is seen in Fig. 5(d). By removing both cross-coupling branches, the PR controller's frequency response becomes symmetrical about dc [12], [15], as shown by its open- and closed-loop responses in Figs. 4(d) and 5(d), respectively. The ability of the PR controller to track positive- and negative-sequence 60-Hz components can be useful in the control of unbalanced systems [15], [16], but compared to the PRX2 controller, this comes at the expense of increased sensitivity to frequency deviations.

B. Experimental Steady-State Time-Domain Analysis

From the previous section, it is apparent that PRX2, PRX$control$, PRX$feedback$, and PR controllers all give zero steady-state error at $+60$ Hz. During balanced operating conditions, the total harmonic distortion of the ac–dc converter loaded at 2 kW is 0.85% for all four stationary frame controllers. Therefore, under balanced operating conditions, the steady-state experimental results of the four controllers are indistinguishable.

More interesting is the response of the various controllers to grid unbalance. An ac–dc converter connected to an unbalanced grid experiences even order harmonics in the dc-link voltage and odd order harmonics in the ac line currents [23]. In the previous section, it was shown that the PRX$feedback$ and PR controllers perfectly track negative-sequence current components. Under an unbalanced grid, this characteristic dramatically influences the ac line current harmonics and dc-link voltage harmonics produced by the converter.

Figs. 6 and 7 show the experimental results of the four stationary frame controllers under a severe 30% drop in phase-C grid voltage e_{Gc}. The PRX$feedback$ and PR controllers display a significantly reduced second harmonic dc ripple component [see Fig. 7(c) and (d)]. This is attributed to the controllers' ability to regulate the negative-sequence line current. Furthermore, due to the reduction of second harmonic dc ripple, a lower third harmonic ac line currents is observed [see Fig. 6(c) and (d)]. Therefore, the line current waveforms for the PRX$feedback$ and PR controllers are noticeably more sinusoidal. In practice, a harmonic filter would be located on the converter side of the PCC in order to limit harmonic injection into the grid and meet IEEE Standard 519. However, in this paper, these filters were omitted to allow for the unencumbered study of controller dynamics.

C. Experimental and Simulation Transient Time-Domain Analysis

Fig. 8 shows the simulated transient response due to a rated dc load step change under balanced grid conditions at nominal 60-Hz frequency (i.e., a 2-kW change to i_{Gd}^{ref}). Fig. 9 shows the related experimental transient response under the same conditions. While the simulation and transient results are similar, the discussion below focuses on the simulation response of Fig. 8 due to the clarity of the waveforms (i.e., less high-order

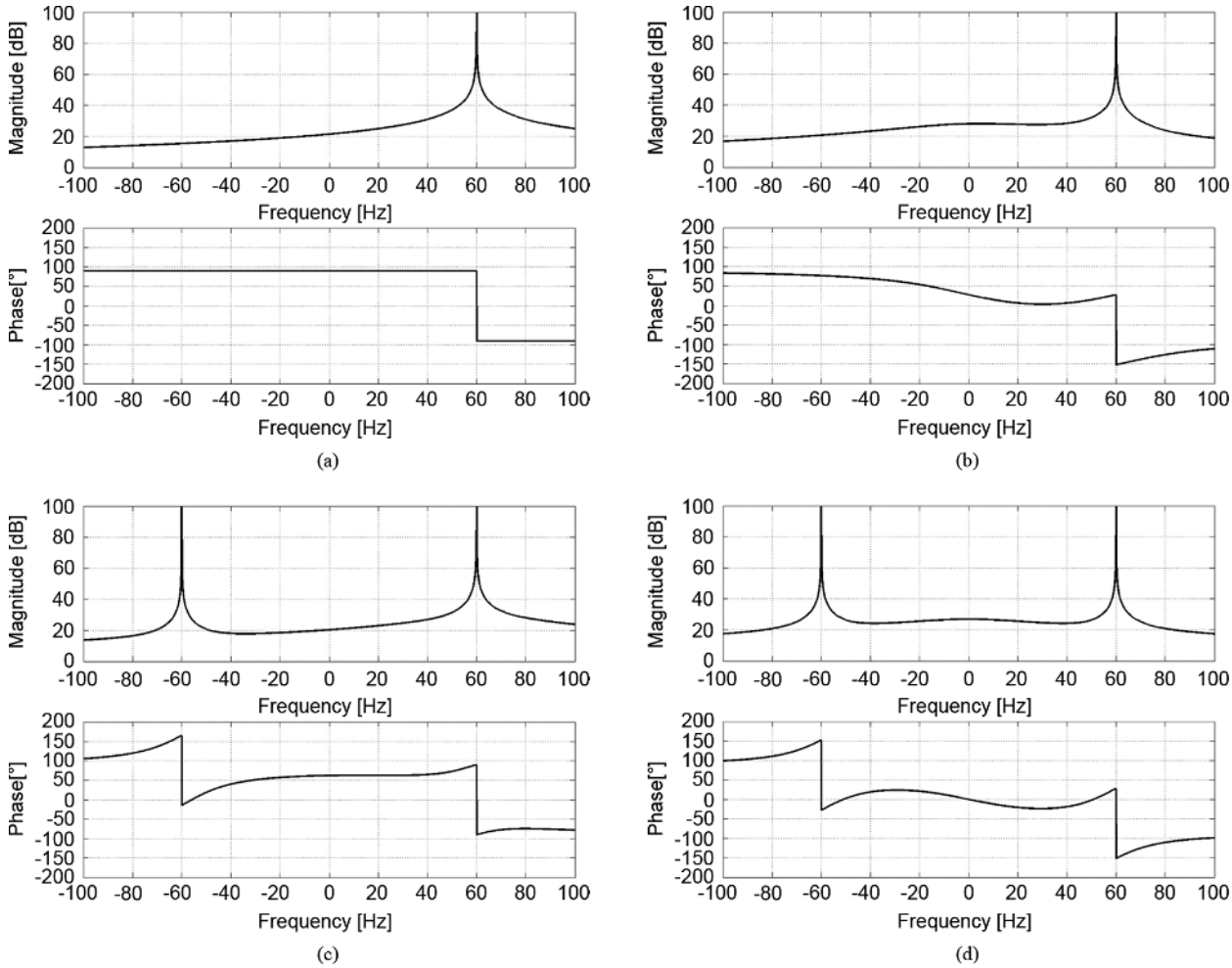

Fig. 4. Complex open-loop frequency response of the stationary frame controllers outlined in Table I. Upper: magnitude; lower: phase response. (a) PRX2 controller. (b) $\mathrm{PRX}control$ controller. (c) $\mathrm{PRX}feedback$ controller. (d) PR controller.

switching harmonic distortion and triggering the load at the same point in the ac voltage cycle). Also, the PCC voltage waveform is superimposed on the line current in Fig. 8 to show that the unity power factor is achieved for all four controllers.

The $\mathrm{X}feedback$ branch is seen to have a negligible effect on the response [see Fig. 8(a) and (b)]. This is in contrast to the dq-frame controller where the associated $j\omega L_K$ decoupling term plays an important role in the system dynamics. Challenges associated with dq-frame decoupling that arise from the feedback filter, antialiasing filter, and other propagation delays [3] are thereby avoided. If only balanced 60-Hz operation in a strongly regulated network is of concern, neglecting the two cross-coupling branches is viable, leading to the conventional PR control structure.

IV. Robustness of Stationary Frame Controllers To Frequency Deviation

The utility system produces grid voltages that deviate from 60 Hz. In developed countries, this frequency deviation is often less than ± 1 Hz [24], [25].

Frequency deviations do not affect the synchronous frame PI controller, as a PLL always ensures controller synchronization. The same cannot be said definitively for the stationary frame controllers presented.

By examining the closed-loop frequency responses of the four stationary frame controllers (see Fig. 5), the robustness of each controller to frequency deviation can be determined. Table III summarizes the maximum and minimum deviation of the closed-loop gain. All four controllers have less than $\pm 2\%$ steady-state error if the fundamental frequency deviates ± 5 Hz, but for large frequency deviations, only the PRX2 controller is able to maintain near unity gain. The greater insensitivity of the PRX2 controller to frequency deviations is strongly correlated to the presence of the $\mathrm{X}feedback$ branch; Its removal in the $\mathrm{PRX}control$ controller causes a much faster deviation from the closed-loop unity gain as outlined in Table III and shown in Fig. 5(a) and (b).

Although converters connected to large utilities would not experience frequency deviations greater than a few Hertz, converters utilized in aerospace or in small remote grids could benefit greatly from the high level of robustness to frequency deviations offered by the PRX2 controller.

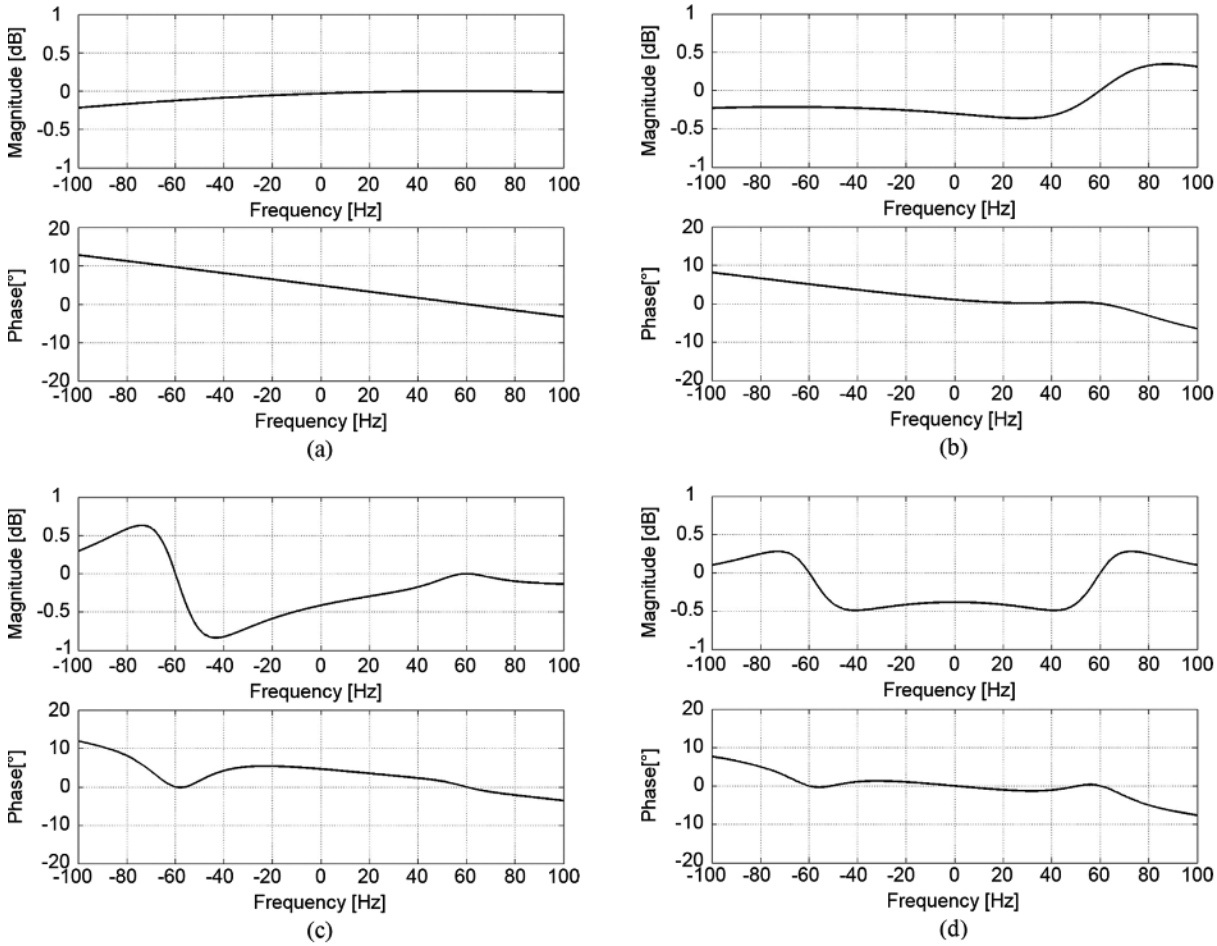

Fig. 5. Complex closed-loop frequency response of stationary frame controllers outlined in Table I; Upper: magnitude; lower: phase response. (a) PRX2 controller. (b) $\mathrm{PRX}control$ controller. (c) $\mathrm{PRX}feedback$ controller. (d) PR controller.

V. Conclusion

This paper expands upon the knowledge of stationary frame-current controllers with resonant components. In doing so, a new stationary frame controller for grid-connected ac-dc converters was introduced that is the exact equivalent of the synchronous frame PI controller with ωL decoupling. The controller is derived by converting the entire synchronous frame model of an ac–dc converter (i.e., converter, controller, and decoupling branches) into the stationary frame. The stationary frame model is then decomposed into two sections—one related to the converter dynamics and the other related to the controller dynamics. This results in the identification of a new stationary frame resonant controller, called the PRX2 controller. The PRX2 controller consists of a proportional (P), resonant (R), and two cross-coupled ($\mathrm{X}control$ and $\mathrm{X}feedback$) components.

The PRX2 controller is unlike other stationary frame controllers containing resonant components because it contains the $\mathrm{X}feedback$ component that is a remnant of the decoupling scheme from the synchronous frame. It is shown that ignoring the $\mathrm{X}feedback$ component greatly increases the controller's sensitivity to frequency deviation about 60 Hz. Therefore, in applications where a high level of robustness to frequency deviation is required, the PRX2 controller should be utilized over other stationary frame resonant controllers.

It has been shown in this paper and by other researchers, that removal of the $\mathrm{X}control$ component causes the controller to regulate negative-sequence currents. It has been experimentally validated that this can have a great impact on systems with grid unbalance to minimize low-order harmonics and for controllers that require negative-sequence control for unbalance compensation.

Several different stationary frame controllers may be derived from the PRX2 controller. In particular, removing both cross-coupling branches in the PRX2 controller produces the familiar stationary frame PR controller. For operation in electrical networks where the grid frequency is tightly regulated, the elimination of these cross-coupling branches is shown to have a negligible effect on dynamic performance. Therefore, controller simplicity is thereby achieved without compromising performance.

Appendix
Proof of Equivalence of the dq and $\alpha\beta$-Frame Models

Synchronous dq-Frame Model With Rotational Transforms: From Fig. 2, the closed-loop transfer function of the synchronous dq-frame model, from the input $\vec{I}^{\mathrm{ref}}_{Gdq}(s)$ to

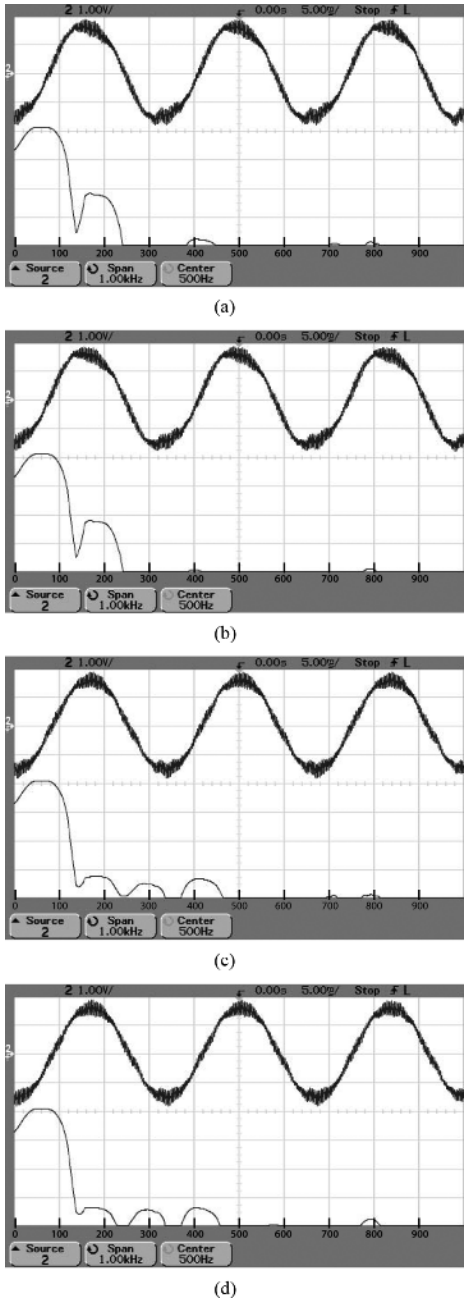

Fig. 6. Experimental steady-state response of phase-A line current to rated loading under 30% phase-C grid voltage drop. Upper: phase-A line current i_{Ga} (vertical axis: 5-A/div attenuation; horizontal axis: 5 ms/div). Lower: amplitude spectrum of phase-A line current i_{Ga}, (vertical axis: 10-dBV/div attenuation, 0-dBV offset. Horizontal axis: 100 Hz/div). (a) PRX2 controller. (b) $\mathrm{PRX}control$ controller. (c) $\mathrm{PRX}feedback$ controller. (d) PR controller.

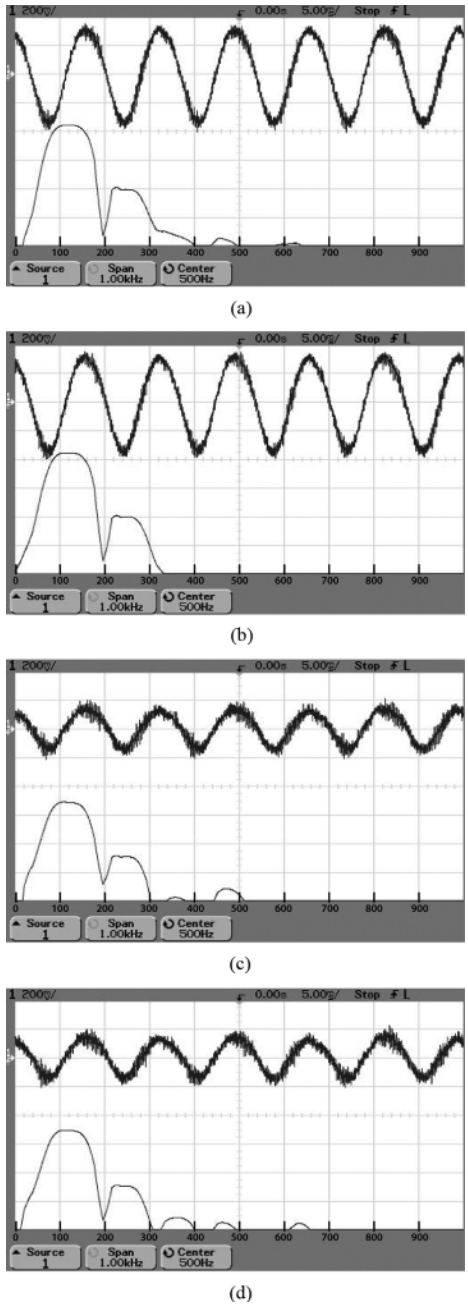

Fig. 7. Experimental steady-state response of dc-link voltage to rated loading under 30% phase-C grid voltage drop. Upper: dc-link voltage u_d, (vertical axis: 14-V/div attenuation; horizontal axis: 5 ms/div). Lower: amplitude spectrum of dc-link voltage u_d^{ripple}, (vertical axis: 10-dBV/div attenuation, -15-dBV offset; horizontal axis: 100 Hz/div). (a) PRX2 controller. (b) $\mathrm{PRX}control$ controller. (c) $\mathrm{PRX}feedback$ controller. (d) PR controller.

output $\vec{I}_{Gdq}(s)$ with the back-emf disturbance set to zero (i.e., $\vec{U}_{Gdq}(s) = 0$) is shown

$$T_{dq}(s) = \left.\frac{\vec{I}_{Gdq}(s)}{\vec{I}^{ref}_{Gdq}(s)}\right|_{\vec{U}_{Gdq}=0} = \frac{\left(\frac{sK_P+K_I}{s}\right)\left(\frac{1}{sL_K+R_K}\right)}{1+\left(\frac{sK_P+K_I}{s}\right)\left(\frac{1}{sL_K+R_K}\right)} = \frac{sK_P+K_I}{s^2L_K+s(R_K+K_P)+K_I}. \quad \text{(A1)}$$

Now, the effect of the rotational transforms in Fig. 2 is examined by analyzing the dq-to-$\alpha\beta$ transformation and its associated Laplace transform [26]. Let $\vec{x}_{dq}(t)$ and $\vec{x}_{\alpha\beta}(t)$ be dq and $\alpha\beta$ space vectors, respectively, related via the dq-to-$\alpha\beta$ transformation [20], and $\vec{X}_{dq}(s)$ and $\vec{X}_{\alpha\beta}(s)$ are their Laplace transforms. The Laplace transform relation of the dq-to-$\alpha\beta$ transformation is [26]

$$\vec{x}_{\alpha\beta}(t) = \vec{x}_{dq}(t)e^{j\omega_N t} \overset{\mathcal{L}}{\longleftrightarrow} \vec{X}_{\alpha\beta}(s) = \vec{X}_{dq}(s - j\omega_N) \quad \text{(A2)}$$

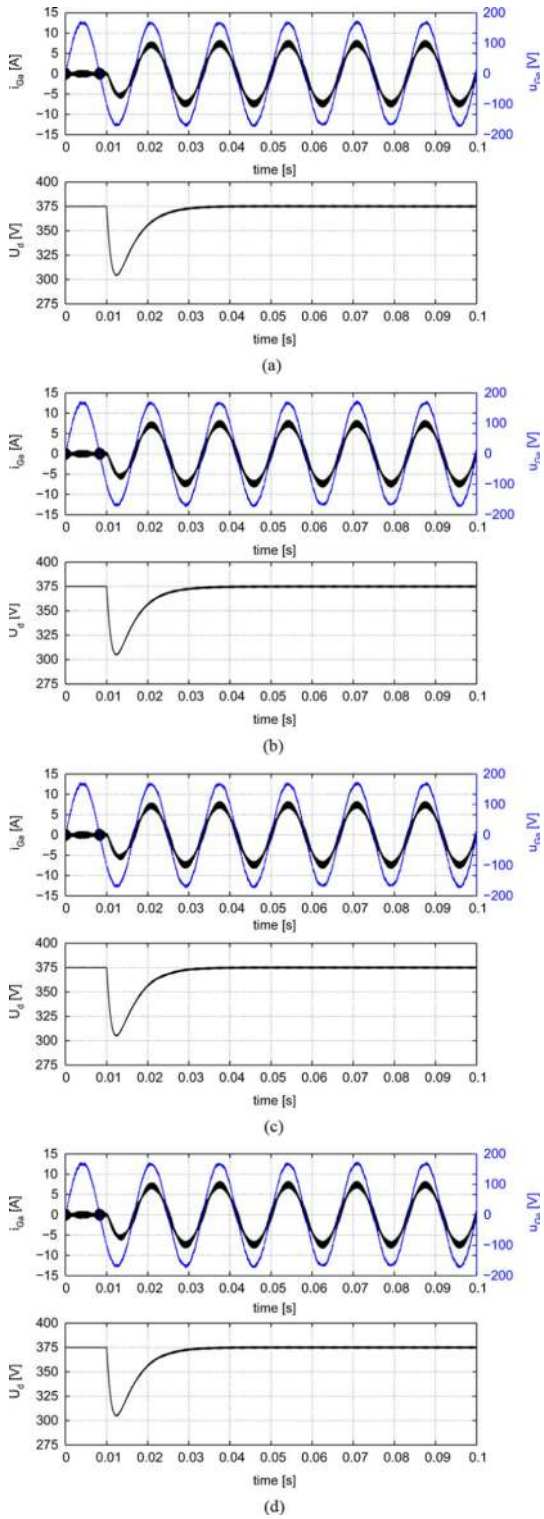

Fig. 8. Simulation transient response of phase-A line current, line-to-neutral phase-A voltage, and dc-link voltage to 2-kW load step change. Upper: phase-A line current i_{Ga} and phase-A line-to-neutral PCC voltage u_{Ga}. Lower: dc-link voltage u_d. (a) PRX2 controller. (b) $\mathrm{PRX}control$ controller. (c) $\mathrm{PRX}feedback$ controller. (d) PR controller.

so that (A3) and (A4) are

$$\vec{i}^{\,\mathrm{ref}}_{G\alpha\beta}(t) = \vec{i}^{\,\mathrm{ref}}_{Gdq}(t)e^{j\omega_N t} \overset{\mathcal{L}}{\longleftrightarrow} \vec{I}^{ref}_{G\alpha\beta}(s) = \vec{I}^{\mathrm{ref}}_{Gdq}(s - j\omega_N) \quad \text{(A3)}$$

$$\vec{i}_{G\alpha\beta}(t) = \vec{i}_{Gdq}(t)e^{j\omega_N t} \overset{\mathcal{L}}{\longleftrightarrow} \vec{I}_{G\alpha\beta}(s) = \vec{I}_{Gdq}(s - j\omega_N). \quad \text{(A4)}$$

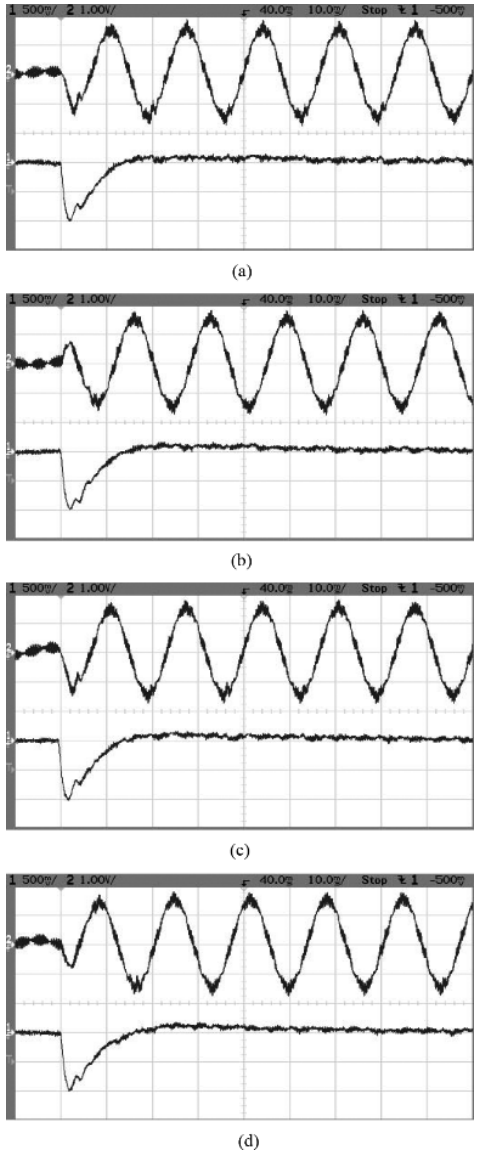

Fig. 9. Experimental transient response of phase-A line current and dc-link voltage to 2-kW load step change. Upper: phase-A line current i_{Ga}, 5-A/div attenuation. Lower: dc-link voltage u_d, 35 V/div attenuation. Horizontal axis: 10 ms/div. (a) PRX2 controller. (b) $\mathrm{PRX}control$ controller. (c) $\mathrm{PRX}feedback$ controller. (d) PR controller.

TABLE III
EFFECT OF FREQUENCY DEVIATION ON THE CLOSED-LOOP GAIN

Controller	**Max and Min Closed Loop Gain Variation for 55 Hz to 65 Hz**	**Frequency Spread for $\pm 2\%$ Closed Loop Gain Change about 60 Hz**
PRX2	-2.5×10^{-4} dB to 0 dB	-80 Hz to 200 Hz
PRX$control$	-0.12 dB to 0.12 dB	52 Hz to 67 Hz
PRX$feedback$	-0.20 dB to 0 dB	40 Hz to 145 Hz
PR	-0.24 dB to 0.19 dB	56 Hz to 65 Hz

From (A3) and (A4), the full $\alpha\beta$-frame transfer function $T_{dq2\alpha\beta}(s)$ from the input $\vec{I}^{\mathrm{ref}}_{G\alpha\beta}(s)$ to the output $\vec{I}_{G\alpha\beta}(s)$ in Fig. 2 is shown

$$T_{dq2\alpha\beta}(s) = \left.\frac{\vec{I}_{G\alpha\beta}(s)}{\vec{I}^{ref}_{G\alpha\beta}(s)}\right|_{\vec{U}_{G\alpha\beta}=0} = \left.\frac{\vec{I}_{Gdq}(s - j\omega_N)}{\vec{I}^{ref}_{Gdq}(s - j\omega_N)}\right|_{\vec{U}_{Gdq}=0} = T_{dq}(s - j\omega_N). \quad \text{(A5)}$$

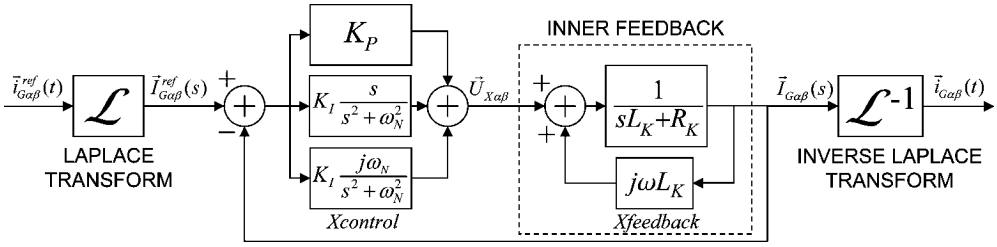

Fig. 10. Stationary $\alpha\beta$-frame model of Fig. 3, where the disturbance $\vec{U}_{\alpha\beta}(s)$ is set to zero and the $\mathrm{X}feedback$ branch is repositioned to aid in the determination of the closed-loop transfer function (A7)–(A10).

where $T_{dq}(s-j\omega_N)$ is determined from (A1) so that the full $\alpha\beta$-frame transfer function is

$$T_{dq2\alpha\beta}(s)=\frac{(s-j\omega_N)K_P+K_I}{(s-j\omega_N)^2L_K+(s-j\omega_N)(R_K+K_P)+K_I}. \tag{A6}$$

Stationary $\alpha\beta$-Frame Model: Examining the stationary $\alpha\beta$-frame model of Fig. 3, the derivation of the closed-loop transfer function from the input $\vec{I}^{ref}_{G\alpha\beta}(s)$ to the output $\vec{I}_{G\alpha\beta}(s)$ with the back-emf disturbance set to zero (i.e., $\vec{U}_{G\alpha\beta}=0$) is made simpler with the block manipulation shown in Fig. 10. The transfer function of the inner feedback loop of Fig. 10 is shown as

$$\begin{aligned}T_{inner}(s)&=\left.\frac{\vec{I}_{G\alpha\beta}(s)}{\vec{U}_{X\alpha\beta}(s)}\right|_{\vec{U}_{G\alpha\beta}=0}=\frac{\frac{1}{sL_K+R_K}}{1-\left(\frac{1}{sL_K+R_K}\right)(j\omega_N L_K)}\\&=\frac{1}{(s-j\omega_N)L_K+R_K}\end{aligned} \tag{A7}$$

where the negative sign in the denominator of the first line is due to the positive feedback loop. The bottom line of (A7) can be interpreted as a frequency-shifted ac plant model when compared to the ac plant model in Fig. 3.

Now, the total forward path $G_{\alpha\beta}(s)$ and feedback path $H_{\alpha\beta}(s)$ of Fig. 10 are

$$\begin{aligned}G_{\alpha\beta}(s)&=G_{PRXcontrol}(s)\,T_{inner}(s)\\&=\left(K_P+K_I\frac{1}{s-j\omega_N}\right)\\&\quad\times\left(\frac{1}{(s-j\omega_N)L_K+R_K}\right)\end{aligned} \tag{A8}$$

$$H_{\alpha\beta}(s)=1 \tag{A9}$$

where $G_{PRXcontrol}(s)$ is taken from (6) in Section II-B.

The $\alpha\beta$-frame closed-loop transfer function is shown

$$\begin{aligned}T_{\alpha\beta}(s)&=\left.\frac{\vec{I}_{G\alpha\beta}(s)}{\vec{I}^{ref}_{G\alpha\beta}(s)}\right|_{\vec{U}_{G\alpha\beta}=0}=\frac{G_{\alpha\beta}(s)}{1+G_{\alpha\beta}(s)H_{\alpha\beta}(s)}\\&=\frac{(s-j\omega_N)K_P+K_I}{(s-j\omega_N)^2L_K+(s-j\omega_N)(R_K+K_P)+K_I}\\&=T_{dq2\alpha\beta}(s)\end{aligned} \tag{A10}$$

which is equal to (A6), which is the transfer function of the synchronous frame model of Fig. 2.

Therefore, in the dq-frame, the input and output time-domain signals are acted upon by the $e^{\pm j\omega_N t}$ modulator, while in the $\alpha\beta$-frame, the frequency-domain controller and plant models are frequency shifted by $j\omega_N$. Both have the same effect as the dq-frame input, and output signals are frequency shifted by ω_N to dc and the model is centered about dc, while the $\alpha\beta$-frame does the opposite and centers the model about $s=j\omega_N$, acting upon the signals at their fundamental frequency.

REFERENCES

[1] N. R. Zargari and G. Joos, "Performance investigation of a current-controlled voltage-regulated PWM rectifier in rotating and stationary frames," *IEEE Trans. Ind. Electron.*, vol. 42, no. 4, pp. 396–401, Aug. 1995.

[2] C. Schauder and H. Mehta, "Vector analysis and control of advanced static VAR compensators," *Proc. Inst. Elect. Eng., Gen., Transm. Distrib.*, vol. 140, no. 4, pp. 299–306, Jul. 1993.

[3] B. Blazic and I. Papic, "Improved D-StatCom control for operation with unbalanced currents and voltages," *IEEE Trans. Power Del.*, vol. 21, no. 1, pp. 225–233, Jan. 2006.

[4] A. Sonnenmoser and P. W. Lehn, "Line current balancing with a unified power flow controller," *IEEE Trans. Power Del.*, vol. 14, no. 3, pp. 1151–1157, Jul. 1999.

[5] A. Yazdani and R. Iravani, "A unified dynamic model and control for the voltage-sourced converter under unbalanced grid conditions," *IEEE Trans. Power. Del*, vol. 21, no. 3, pp. 1620–1629, Jul. 2006.

[6] C. K. Sao, P. W. Lehn, M. R. Iravani, and J. A. Martinez, "A benchmark system for digital time-domain simulation of a pulse-width-modulated D-STATCOM," *IEEE Trans. Power Del.*, vol. 17, no. 4, pp. 1113–1120, Oct. 2002.

[7] B.-S. Chen and Y.-Y. Hsu, "An analytical approach to harmonic analysis and controller design of a STATCOM," *IEEE Trans. Power Del.*, vol. 22, no. 1, pp. 423–432, Jan. 2007.

[8] K. R. Padiyar and N. Prabhu, "Design and performance evaluation of subsynchronous damping controller with STATCOM," *IEEE Trans. Power Del.*, vol. 21, no. 3, pp. 1398–1405, Jul. 2006.

[9] D. N. Zmood, "A systematic development of improved linear regulators for sinusoidal power converters," Ph.D. dissertation, Monash University, Clayton, Victoria, Australia, 2002.

[10] D. N. Zmood, D. G. Holmes, and G. H. Bode, "Frequency-domain analysis of three-phase linear current regulators," *IEEE Trans. Ind. Appl.*, vol. 37, no. 2, pp. 601–610, Mar./Apr. 2001.

[11] D. N. Zmood and D. G. Holmes, "Stationary frame current regulation of PWM inverters with zero steady-state error," *IEEE Trans. Power Electron.*, vol. 18, no. 3, pp. 814–822, May 2003.

[12] X. Yuan, W. Merk, H. Stemmler, and J. Allmeling, "Stationary-frame generalized integrators for current control of active power filters with zero steady-state error for current harmonics of concern under unbalanced and distorted operating conditions," *IEEE Trans. Ind. Appl.*, vol. 38, no. 2, pp. 523–532, Mar./Apr. 2002.

[13] B. A. Francis and W. M. Wonham, "The internal model principle for linear multivariable regulators," *J. Appl. Maths. Optim.*, vol. 2, no. 2, pp. 170–194, 1975.

[14] J.-W. G. Hwang, M. Winkelnkemper, and P. W. Lehn, "Design of an optimal stationary frame controller for grid connected ac-dc converters," in *Proc. IEEE 32nd Annu. Conf. Industrial Electronics Soc.*, Paris, France, Nov. 2006, pp. 167–172.

[15] F. Blaabjerg, R. Teodorescu, M. Liserre, and A. V. Timbus, "Overview of control and grid synchronization for distributed power generation systems," *IEEE Trans. Ind. Electron.*, vol. 53, no. 5, pp. 1398–1409, Oct. 2006.

[16] J. G. Hwang, P. W. Lehn, and M. Winkelnkemper, "Control of grid connected ac-dc converters with minimized dc link capacitance under unbalanced grid voltage condition," in *Proc. Eur. Conf. Power Electronics and Applications*, Aalborg, Denmark, Sep. 2007, pp. 1–10.

[17] Y. Jiang and Å Ekström, "Applying PWM to control overcurrents at unbalanced faults of forced-commutated VSCs used as static var compensators," *IEEE Trans. Power Del.*, vol. 12, no. 1, pp. 273–278, Jan. 1997.

[18] H.-S. Song and K. Nam, "Dual current control scheme for PWM converter under unbalanced input voltage conditions," *IEEE Trans. Ind. Electron.*, vol. 46, no. 5, pp. 953–959, Oct. 1999.

[19] C. Sao and P. W. Lehn, "A block diagram approach to reference frame transformation of converter dynamic models," in *Proc. Canadian Conf. Electrical and Computer Engineering*, Ottawa, ON, Canada, May 2006, pp. 2270–2274.

[20] P. C. Krause, O. Wasynczuk, and S. D. Sudhoff*, Analysis of Electric Machinery and Drive Systems*. New York: Wiley-IEEE Press, 2002.

[21] H. Kömürcügil and O. Kükrer, "Lyapunov-based control for three-phase PWM ac/dc voltage-source converters," *IEEE Trans. Power Electron.*, vol. 13, no. 5, pp. 801–813, Sep. 1998.

[22] I. Papic and P. Zunko, "UPFC converter-level control system using internally calculated quantities for decoupling," *Int. J. Elect. Power Energy Syst.*, no. 25, pp. 667–675, 2003.

[23] L. Morán and P. D. Ziogas, "Design aspects of synchronous PWM rectifier-inverter systems under unbalanced input voltage conditions," *IEEE Trans. Ind. Appl.*, vol. 28, no. 6, pp. 1286–1293, Nov./Dec. 1992.

[24] *IEEE Recommended Practice for Utility Interface of Photovoltaic (PV) Systems,* , IEEE Std. 929-2000, IEEE., New York.

[25] *, Standards for Inverters, Converters, and Controllers for use in Independent Power Systems*, UL 1741, Std. 1741, Underwriters Laboratories, Inc., Northbrook, IL.

[26] A. V. Oppenheim, A. S. Willsky, and S. H. Nawab*, Signals & Systems*, 2nd ed. Englewood Cliffs, NJ: Prentice-Hall, 1997.

J. George Hwang (S'04) received the B.A.Sc. and M.A.Sc. degrees in electrical engineering from the University of Toronto, Toronto, ON, Canada, in 2004 and 2007, respectively, and is currently pursuing the Ph.D. degree at the Massachusetts Institute of Technology, Cambridge.

From 2005 to 2006, he was with the Power Electronics Systems Group, ABB Corporate Research Center, Baden, Switzerland. Prior to that, he was with the Systems Integration Group, Hydrogenics Corporation, Mississauga, ON, Canada, working on fuel-cell power systems. His research interests include modeling and control of converters and high-voltage charge transport and breakdown phenomena in dielectrics.

Peter W. Lehn (SM'05) received the B.Sc. and M.Sc. degrees in electrical engineering from the University of Manitoba, Winnipeg, MB, Canada, in 1990 and 1992, respectively, and the Ph.D. degree from the University of Toronto, Toronto, ON, Canada, in 1999.

From 1992 to 1994, he was with the Network Planning Group, Siemens AG, Erlangen, Germany. Currently, he is a Professor with the University of Toronto. His research interests include modeling and control of converters and integration of renewable energy sources into the power grid.

Manfred Winkelnkemper (M'05) received the Dipl.-Ing. and Ph.D. degrees in electrical engineering from the University of Technology, Berlin, Germany, in 1998 and 2005, respectively.

From 2004 to 2008, he was with the Power Electronics Systems Group, ABB Corporate Research Center, Baden, Switzerland. Currently, he is a Senior R&D Engineer for Medium Voltage Drives in ABB Automation Products, Switzerland.